

From Electrons to Finite Elements: A Concurrent Multiscale Approach for Metals

Gang Lu⁽¹⁾, E. B. Tadmor⁽²⁾ and Efthimios Kaxiras⁽³⁾

⁽¹⁾*Department of Physics and Astronomy, California State University Northridge, Northridge, California 91330*

⁽²⁾*Department of Mechanical Engineering, Technion – Israel Institute of Technology, 32000 Haifa, Israel*

⁽³⁾*Department of Physics and Division of Engineering and Applied Sciences, Harvard University, Cambridge, Massachusetts 02138*

(Dated: October 6, 2018)

We present a multiscale modeling approach that concurrently couples quantum mechanical, classical atomistic and continuum mechanics simulations in a unified fashion for metals. This approach is particularly useful for systems where chemical interactions in a small region can affect the macroscopic properties of a material. We discuss how the coupling across different scales can be accomplished efficiently, and we apply the method to multiscale simulations of an edge dislocation in aluminum in the absence and presence of H impurities.

Some of the most fascinating problems in all fields of science involve multiple spatial and/or temporal scales: processes that occur at a certain scale govern the behavior of the system across several (usually larger) scales. In the context of materials science, the ultimate microscopic constituents of materials are ions and valence electrons; interactions among them at the atomic level determine the behavior of the material at the macroscopic scale, the latter being the scale of interest for technological applications. Conceptually, two categories of multiscale simulations can be envisioned, sequential, consisting of passing information across scales, and concurrent, consisting of seamless coupling of scales [1]. The majority of multiscale simulations that are currently in use are sequential ones, which are effective in systems where the different scales are weakly coupled. For systems whose behavior at each scale depends strongly on what happens at the other scales, concurrent approaches are usually required. In contrast to sequential approaches, concurrent simulations are still relatively new and only a few models have been developed to date [1, 2, 3, 4, 5, 6].

A successful concurrent multiscale method is the Quasicontinuum (QC) method originally proposed by Tadmor et al. [2]. The idea underlying this method is that atomistic processes of interest often occur in very small spatial domains while the vast majority of atoms in the material behave according to well-established continuum theories. To exploit this fact, the QC method retains atomic resolution only where necessary and grades out to a continuum finite element description elsewhere. The original formulation of QC was limited to classical potentials for describing interactions between atoms. Since many materials properties depend *explicitly* on the behavior of electrons, such as bond breaking/forming at crack tips or defect cores, chemical reactions with impurities, and surface reactions and reconstructions, it is desirable to incorporate appropriate quantum mechanical descriptions into the QC formalism. In this Letter, we extend the original QC approach so that it can be directly coupled with quantum mechanical calculations based on density functional theory (DFT) for metallic

systems. We refer to the new approach as QCDFE.

The goal of the QC method is to model an atomistic system without explicitly treating every atom in the problem [2, 7]. This is achieved by replacing the full set of N atoms with a small subset of N_r “representative atoms” or *repatoms* ($N_r \ll N$) that approximate the total energy through appropriate weighting. The energies of individual repatoms are computed in two different ways depending on the deformation in their immediate vicinity. Atoms experiencing large deformation gradients on an atomic-scale are computed in the same way as in a standard fully-atomistic method. In QC these atoms are called *nonlocal* atoms to reflect the fact that their energy depends on the positions of their neighbors in addition to their own position. In contrast, the energies of atoms experiencing a smooth deformation field on the atomic scale are computed based on the deformation gradient in their vicinity as befitting a continuum model. These atoms are called *local* atoms because their energy is based only on the deformation gradient at the point where it is computed. The total energy E_{tot} (which for a classical system can be written as $E_{\text{tot}} = \sum_{i=1}^N E_i$, with E_i the energy of atom i) is approximated as

$$E_{\text{tot}}^{\text{QC}} = \sum_{i=1}^{N^{\text{nl}}} E_i(\{\mathbf{q}\}) + \sum_{j=1}^{N^{\text{loc}}} n_j E_j^{\text{loc}}(\{\mathbf{F}\}). \quad (1)$$

The total energy has been divided into two parts: an atomistic region of N^{nl} nonlocal atoms and a continuum region of N^{loc} local atoms ($N^{\text{nl}} + N^{\text{loc}} = N_r$). The calculation in the atomistic region is identical to that in fully atomistic methods with the energy of the atom depending on the coordinates $\{\mathbf{q}\}$ of the surrounding repatoms. However, in the coarse-grained continuum region each repatom can represent a large region of n_i atoms on the atomic scale. Rather than depending on the positions of neighboring atoms, the energy of a local repatom depends on the deformation gradients $\{\mathbf{F}\}$ characterizing the finite strain around its position. The basic assumption employed is the Cauchy-Born rule which relates the continuum deformation at a point to the motion of the

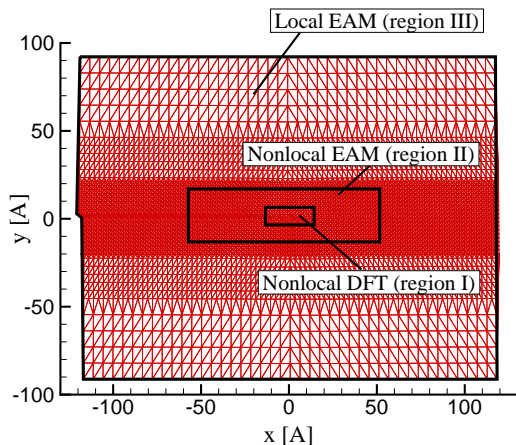


FIG. 1: QCDFD model for an edge dislocation showing the three domains in the model (see text). The x , y and z axes are along $[\bar{1}10]$, $[111]$ and $[11\bar{2}]$, respectively. The model contains about 990 nonlocal atoms of which 84 are in the DFT region, 3700 local atoms and 9300 finite elements. All atoms are initially displaced according to the anisotropic elastic solution of the dislocation with the boundaries held fixed to these values during the relaxation phase. Periodic boundary conditions are applied along the dislocation line (z) direction.

atoms in the underlying lattice represented by this point. To obtain the necessary deformation gradients, a finite element mesh is defined with the representative atoms as its nodes. It is important to note that the calculations of $E_j^{\text{loc}}(\{\mathbf{F}\})$ in the continuum regions make use of the same interatomic potential used in the nonlocal atomistic region. This makes the passage from the atomistic to continuum regions seamless since the same material description is used in both. This seamless description enables the model to adapt automatically to changing circumstances, for example the nucleation of new defects or the migration of existing defects. The adaptability of QC is one of its main strengths, which is missing in many other multiscale methods. A consequence of the partitioning into local and nonlocal regions and the existence of a well-defined total energy for the entire system is the presence of non-physical *ghost forces* at the interface. These can be eliminated by self-consistent application of dead load corrections [7].

The original QC formulation assumes that the total energy can be written as a sum over individual atom energies. This condition is not satisfied by quantum mechanical models. To address this limitation, in the present QCDFD approach the material of interest is partitioned into three distinct types of domains (see Fig. 1): (1) a nonlocal quantum mechanical DFT region (region I); (2) a nonlocal classical region where Embedded-Atom Method (EAM) [8] potentials are used (region II); and (3) a local region that employs the same EAM potentials as region II (region III). The total energy of the QCDFD

system is then

$$E_{\text{tot}}^{\text{QCDFD}} = E[\text{I} + \text{II}] + \sum_{j=1}^{N^{\text{loc}}} n_j E_j^{\text{loc}}(\{\mathbf{F}\}), \quad (2)$$

where $E[\text{I} + \text{II}]$ is the total energy of regions I and II together (the assumption here is that region I is embedded within region II). The coupling between regions II and III is achieved seamlessly via the QC formulation, while the coupling between regions I and II is accomplished by a scheme recently proposed by Choly *et al.* [9]. Based on this coupling strategy, $E[\text{I} + \text{II}]$ can be written as

$$E[\text{I} + \text{II}] = E_{\text{DFT}}[\text{I}] + E_{\text{EAM}}[\text{II}] + E^{\text{int}}[\text{I}, \text{II}], \quad (3)$$

where $E_{\text{DFT}}[\text{I}]$ is the energy of region I in the absence of region II computed using the DFT model, $E_{\text{EAM}}[\text{II}]$ is the energy of region II in the absence of region I computed using the EAM model, and $E^{\text{int}}[\text{I}, \text{II}]$ represents a formal interaction energy added to give the correct total energy. The interaction energy between the two subsystems can be rewritten as:

$$\begin{aligned} E^{\text{int}}[\text{I}, \text{II}] &\equiv E[\text{I} + \text{II}] - E[\text{I}] - E[\text{II}], \\ &= E_{\text{EAM}}[\text{I} + \text{II}] - E_{\text{EAM}}[\text{I}] - E_{\text{EAM}}[\text{II}]. \end{aligned} \quad (4)$$

The first equation serves as a general definition of the interaction energy whereas the second equation represents one particular implementation of E^{int} , which is used in this work. Eq. 4 is not contradictory to Eq. 3 because EAM has its root in DFT and the EAM energy can be viewed as an approximation to the DFT energy. Different combinations of quantum mechanical and classical atomistic methods other than DFT/EAM may also be implemented [9]. The great advantage of the present implementation is its simplicity. It demands nothing beyond what is required for a DFT calculation and an EAM QC calculation. Furthermore, by substituting Eq. 4 into Eq. 3, we arrive at

$$E[\text{I} + \text{II}] = E_{\text{DFT}}[\text{I}] - E_{\text{EAM}}[\text{I}] + E_{\text{EAM}}[\text{I} + \text{II}]. \quad (5)$$

The forces on the EAM atoms in region II are then

$$-\mathbf{F}_i^{\text{II}} = \frac{E_{\text{tot}}^{\text{QCDFD}}}{\partial \mathbf{q}_i^{\text{II}}} = \frac{\partial E_{\text{EAM}}[\text{I} + \text{II}]}{\partial \mathbf{q}_i^{\text{II}}} + \frac{\sum_{j=1}^{N^{\text{loc}}} n_j E_j^{\text{loc}}(\{\mathbf{F}\})}{\partial \mathbf{q}_i^{\text{II}}}, \quad (6)$$

where \mathbf{q}_i^{II} are the Cartesian coordinates of atom i in region II. It is clear from this equation that the forces on the atoms in region II are identical to those that would be obtained from a fully-classical QC calculation. The same applies to the region III atoms, that is, as far as forces are concerned, regions II and III behave as though the entire model were classical. This is a very desirable property in terms of achieving a seamless coupling between region I and the rest of the model. At the same time,

the forces on the DFT atoms in region I will have contributions from both DFT atoms and the nearby EAM atoms in region II. The error in forces on the DFT atoms due to the coupling is thus given by the difference between calculated forces with DFT and EAM on these atoms. To minimize this error, we propose to use a class of interatomic potentials which are generated by matching the forces obtained from the EAM method to those from DFT calculations [10, 11]. Another important practical advantage of the present QCDFD method is that, if region I contains many different atomic species while region II contains only one atom type, there is no need to develop reliable EAM potentials that can describe each species and their interactions. This is because if the various species of atoms are well within region I, then the energy contributions of these atoms are canceled out in the total energy calculation (the last two terms in Eq. 5). This advantage renders the method particularly useful in dealing with impurities, which is an exceedingly difficult task for empirical potential simulations.

The equilibrium structure of the system is obtained by minimizing the total energy in Eq. 2 with respect to all degrees of freedom. Because the time required to evaluate $E_{\text{DFT}}[\mathbf{I}]$ is considerably more than that required for computation of the other EAM terms in $E_{\text{tot}}^{\text{QCDFD}}$, an alternate relaxation scheme turns out to be rather efficient. The total system can be relaxed by using the conjugate gradient approach on the DFT atoms alone, while fully relaxing the EAM atoms in region II and the displacement field in region III at each step. Similar to Choly *et al.* [9], an auxiliary energy function can be defined as

$$E'[\{\mathbf{q}^{\text{I}}\}] \equiv \min_{\{\mathbf{q}^{\text{II}}\}, \{\mathbf{q}^{\text{III}}\}} E_{\text{tot}}^{\text{QCDFD}}[\{\mathbf{q}\}], \quad (7)$$

which allows for the following relaxation scheme: (i) Minimize $E_{\text{tot}}^{\text{QCDFD}}$ with respect to the atoms in regions II ($\{\mathbf{q}^{\text{II}}\}$) and the atoms in region III ($\{\mathbf{q}^{\text{III}}\}$), while holding the atoms in region I fixed; (ii) Calculate $E_{\text{tot}}^{\text{QCDFD}}[\{\mathbf{q}\}]$, and the forces on the region I atoms; (iii) Perform a step of conjugate gradient minimization of E' ; (iv) Repeat until the system is relaxed. In this manner, the number of DFT calculations performed is greatly reduced, albeit at the expense of more EAM and local QC calculations. A number of tests have shown that the total number of DFT energy calculations for the relaxation of an entire system is about the same as that required for DFT relaxation of region I alone. Further computational speed-up can be achieved for the DFT calculations by using converged electronic charge density and wave functions from the previous step, so that the charge (potential) self-consistency can be reached faster for the next DFT calculation because the atomic relaxation is usually very small between two consecutive DFT moves.

In the remainder of the paper, we apply the present QCDFD approach to study the core structure of an edge dislocation in Al in the absence and presence of H impuri-

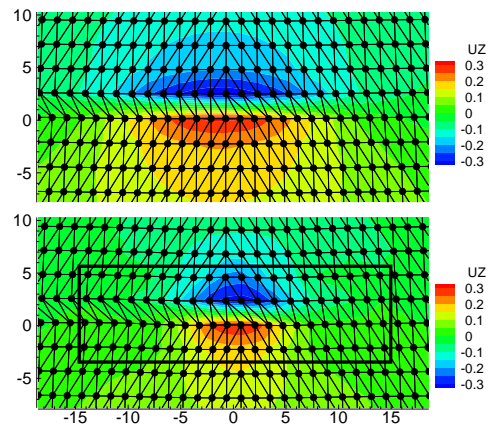


FIG. 2: Dislocation core structures obtained from the EAM-based QC (top) and the present QCDFD method (bottom). The black circles are atoms. The contours correspond to out-of-plane (z) displacement in Å. The contours clearly indicate the splitting of the dislocation. The atoms within the black box in the bottom panel are DFT atoms. The finite element mesh serves no other purpose in this nonlocal atomistic region other than as a guide to the eye to help visualize deformation.

ties. We chose this system as an example because results from both experiments and simulations are available for comparison. The QCDFD model for an edge dislocation with a Burgers vector $\frac{a}{2}[110]$ ($a = 3.97$ Å) is presented in Fig. 1. Convergence tests on the size of region I indicate that a DFT box of 30 Å \times 9 Å \times 4.86 Å (84 DFT atoms) is sufficient to capture the dislocation splitting behavior accurately; hence the following calculations are all based on this DFT box. A force-matching potential for Al [10] was used for EAM calculations. The DFT calculations were performed by using the plane-wave pseudopotential VASP code [12] for a cluster with 8 Å vacuum in both the x and y directions. The energy cutoff for pure Al and Al+H is 129 eV and 200 eV, respectively. We find that 10 k points along the one-dimensional Brillouin zone are adequate for good convergence. Fig. 2 presents the simulation results for both a standard EAM-based QC calculation and the QCDFD method, showing the dissociation of the edge dislocation into two equivalent 60° Shockley partials. The splitting distance (obtained from an analysis of the displacement jump across the slip plane) in the standard QC calculation is 15.4 Å, whereas the splitting distance obtained with QCDFD method is 5.6 Å, a value very close to the experimentally observed value of 5.5 Å [13]. This result demonstrates that even for a simple metal like Al which should be the best candidate for use of an EAM potential, a quantum mechanical calculation is necessary to obtain correct results.

The most important advantage of QCDFD approach, however, is that it allows the study of impurity effects on mechanical response, an impossible task for simpler empirical potentials. Fig. 3 shows the effect of adding one column of H impurities at the dislocation core. The

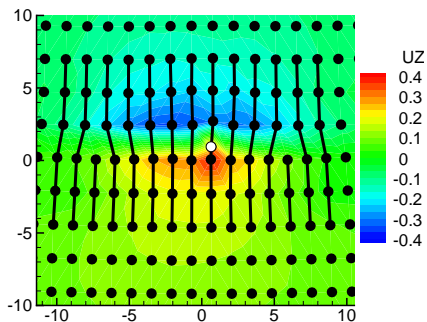


FIG. 3: QCDFD dislocation core structure in the presence of a column of H impurities. The circles are Al atoms (black) and H atom (white). Contour significance is the same as in Fig. 2. The black lines are a guide to the eye, indicating atomic planes.

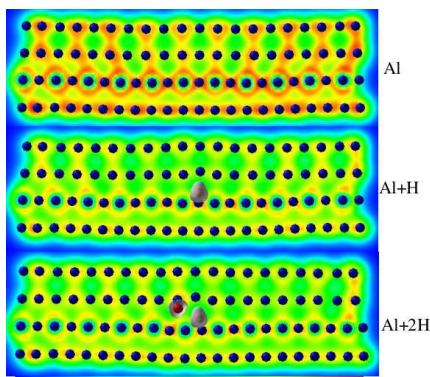


FIG. 4: Charge density distribution in region I in the absence (top) and in the presence of one (middle) and two H impurity atoms (bottom). The blue spheres are Al atoms and the red spheres are H atoms. The gray iso-surfaces illustrate the charge density distribution at $0.28 \text{ electrons}/\text{\AA}^3$. Electron density values range from 0 to $0.30 \text{ electrons}/\text{\AA}^3$.

presence of the H atoms results in a spreading of the core (the splitting distance is now increased to about 13 \AA). This finding is consistent with the fact, confirmed by earlier DFT calculations [14], that H can lower the stacking fault energy. The fact that the dislocation becomes wider may explain the H-enhanced dislocation mobility that is believed to lead to H embrittlement phenomena via the enhanced local plasticity theory. A similar core structure is also found for two columns of H atoms placed at the dislocation core. In order to understand the underlying origin of the H-enhanced dislocation mobility, we calculate the electron density distribution at the dislocation core in the absence and presence of H impurities, as shown in Fig. 4. In the absence of the H impurity, the electron bonding is stronger and with a distinct covalent character. The bonding is more directional above the slip plane, and it becomes more spherical below the slip plane where there are two extra atomic planes, corresponding to the two partial dislocations. In the presence

of H atoms, charge accumulation develops at these H atoms as the H impurities attract the valence electrons from the Al atoms and become negatively charged. The covalent bonding across the slip plane between Al atoms is disrupted by the H atoms, and at the same time, ionic bonding between the oppositely charged H and Al ions is developed. The fact that the directional covalent bonds are replaced by more homogeneous ionic bonds near the core leads to the wider dislocation core seen in Fig. 2.

In summary, we have introduced a multiscale modeling approach which concurrently couples quantum mechanical, classical atomistic and continuum mechanics simulations, in a unified fashion for metals. Our QCDFD method provides a useful framework for multiscale modeling of metallic materials because it does not require the existence of localized covalent bonds for computing the coupling energy as all other multiscale methods do [3, 4, 5, 6]. Furthermore, this approach is completely general and versatile: it can be applied to diverse materials problems, such as dislocations, cracks, surfaces, and grain boundaries. Finally, the automatic adaption feature of the QCDFD method allows the DFT and/or EAM region to move and change in response to the current deformation state, when for example, defects are being nucleated in an otherwise perfect region. To demonstrate the unique strength of this method in dealing with impurities, we have applied it to study H-dislocation interactions in Al.

This research was partly supported by an award from Research Corporation (GL). ET and GL thank the Institute for Mathematics and its Applications (IMA) for hosting them in the fall of 2004 during which time part of this work was done.

-
- [1] G. Lu and E. Kaxiras, in *Handbook of Theoretical and Computational Nanotechnology*, Edited by M. Rieth, and W. Schommers, (American Scientific Publisher, Stevenson Ranch, CA, 2005), Chap. 22
 - [2] E. B. Tadmor, M. Ortiz, and R. Phillips, *Philos. Mag. A* **73**, 1529 (1996).
 - [3] J. Gao, *Rev. Compt. Chem.* **7**, 119 (1996).
 - [4] J. Broughton *et al.*, *Phys. Rev. B* **60**, 2391 (1999).
 - [5] N. Bernstein and D. Hess, *Mat. Res. Soc. Symp. Proc.* **653**, Z2.7.1 (2001).
 - [6] E. Lidorikis, *et al.*, *Phys. Rev. Lett.* **87**, 086104 (2001).
 - [7] V. B. Shenoy *et al.*, *J. Mech. Phys. Solids* **47**, 611 (1999).
 - [8] M. S. Daw and M. I. Baskes, *Phys. Rev. B* **29**, 6443 (1984).
 - [9] N. Choly *et al.*, *Phys. Rev. B* **71**, 094101 (2005).
 - [10] F. Ercolessi and J. B. Adams, *Europhys. Lett.* **26**, 583 (1994).
 - [11] Y. Li *et al.*, *Phys. Rev. B* **67**, 125101 (2003).
 - [12] G. Kresse and J. Furthmüller, *Phys. Rev. B* **54**, 11166 (1996).
 - [13] M. Mills and P. Stadelmann, *Philos. Mag. A* **60**, 355 (1989).

[14] G. Lu *et al.*, Phys. Rev. Lett. **87**, 095501 (2001).